Published in final edited form as:
Proteomics. 2011 October ; 11(19): 3853–3865. doi:10.1002/pmic.201100253.

IDENTIFICATION AND REMOVAL OF PROTEINS THAT CO-PURIFY WITH INFECTIOUS PRION PROTEIN IMPROVES THE ANALYSIS OF ITS SECONDARY STRUCTURE

Roger A. Moore[1,2,*], **Andrew Timmes**[1,2], **Phillip A. Wilmarth**[3], **David Safronetz**[4], and **Suzette A. Priola**[1]

[1]Rocky Mountain Laboratories, National Institute of Allergy & Infectious Disease, Laboratory of Persistent Viral Disease National Institutes of Health

[4]Laboratory of Virology, National Institutes of Health

[3]Department of Biochemistry and Molecular Biology, School of Medicine, Oregon Health & Science University

Abstract

Prion diseases are neurodegenerative disorders associated with the accumulation of an abnormal isoform of the mammalian prion protein (PrP). Fourier transform infrared spectroscopy (FTIR) has previously been used to show that the conformation of aggregated, infectious PrP (PrP^{Sc}) varies between prion strains and these unique conformations may determine strain-specific disease phenotypes. However, the relative amounts of α-helix, β-sheet and other secondary structures have not always been consistent between studies suggesting that other proteins might be confounding the analysis of PrP^{Sc} secondary structure. We have used FTIR and tandem mass spectrometry to analyze enriched PrP^{Sc} from mouse and hamster prion strains both before and after the removal of protein contaminants that commonly co-purify with PrP^{Sc}. Our data show that non-PrP proteins do contribute to absorbances that have been associated with α-helical, loop, turn, and β-sheet structures attributed to PrP^{Sc}. The major contaminant, the α-helical protein ferritin, absorbs strongly at 1652cm^{-1} in the FTIR spectrum associated with PrP^{Sc}. However, even the removal of greater than 99% of the ferritin from PrP^{Sc} did not completely abolish absorbance at 1652cm^{-1}. Our results show that contaminating proteins alter the FTIR spectrum attributed to PrP^{Sc} and suggest that the α-helical, loop/turn, and β-sheet secondary structure that remains following their removal are derived from PrP^{Sc} itself.

Keywords

Transmissible spongiform encephalopathies; TSE; Prion protein; FTIR; infrared spectroscopy; LC-MS/MS; scrapie; proteomics; secondary structure; 79A; 22A; 263K; ferritin; apolipoprotein E

Transmissible spongiform encephalopathies (TSEs), or prion diseases are fatal, neurodegenerative diseases that include Creutzfeldt-Jakob disease in humans, scrapie in

[*]Correspondence: Roger A. Moore, Ph.D. National Institutes of Health National Institute of Allergy & Infectious Disease Laboratory of Persistent Viral Disease Rocky Mountain Laboratories 903 S. 4th Str. Hamilton, MT 59840 Tel: 406-363-9391 Fax: 406-363-9286 rmoore@niaid.nih.gov.
[2]These authors contributed equally

Conflict of Interest. The authors declare no conflict of interest.

Supporting Information. Two supplemental figures, a supplemental table and complete lists of peptides are available as Excel worksheets.

sheep, chronic wasting disease in deer and elk and bovine spongiform encephalopathy in cattle (1). The conformational conversion of soluble, protease-sensitive mammalian prion protein (PrP^C) from a structure rich in α-helix to an insoluble, protease-resistant form that is rich in β-sheet (PrP^{Sc}) is a critical event in prion disease pathogenesis (2). Prion diseases are unique among protein misfolding disorders in that they are transmissible (1). PrP^{Sc} is believed to be the primary component of the prion infectious agent and the molecular basis of prion diseases is likely to be at least in part determined by specific PrP^{Sc} conformations (3–7) which lead to different prion strains exhibiting characteristic phenotypes in vivo (2;8). In order to understand how PrP^{Sc} conformation may influence disease phenotype in vivo, it is important to determine the structure of PrP^{Sc} from different prion strains.

The structural differences between naturally occurring PrP^C and PrP^{Sc} are remarkable, given that they share the same primary amino acid sequence. The structure of PrP^C has been studied in detail by high resolution NMR spectroscopy (9–11) and, to a lesser extent, by X-ray crystallography (12). These data cumulatively show that PrP^C is approximately 47% α-helical, 3% β-strand and contains a natively unstructured N-terminus (9). By contrast, because PrP^{Sc} is highly aggregated and difficult to purify to homogeneity, no high resolution structures have been determined. Lower resolution techniques such as circular dichroism (13), fourier-transform infrared spectroscopy (FTIR) (14–16), and hydrogen-deuterium exchange (17) have established that PrP^{Sc} aggregates contain much more β-sheet secondary structure compared to monomeric PrP^C. Most of the current literature suggests that PrP^{Sc} retains some portion of its pre-conversion α-helix content when converted to PrP^{Sc} (2;18;19), although other studies suggest that PrP^{Sc} retains no α-helix character at all (13;16;17). These discrepancies could be explained by the presence of contaminating proteins that co-purify with PrP^{Sc}. Various protocols for PrP^{Sc} enrichment developed over the last three decades (20–24) have yielded PrP^{Sc} samples which are actually complex mixtures that can contain carbohydrates (25), lipids (26), nucleic acids (27), other proteins (28;29), and probably metal ions (30). However, no structural study has directly addressed how these contaminants might contribute to structural features attributed to PrP^{Sc}.

Using an improved PrP^{Sc} purification protocol, we have examined the secondary structure of mouse and hamster PrP^{Sc} both before and after the removal of major protein contaminants that commonly co-purify with PrP^{Sc}. Tandem mass spectrometry (LC-MS/MS) was used to identify the proteins in our samples while FTIR was used to probe secondary structure. The results show that non-PrP proteins do contribute to absorbance associated with α-helical, loop, turn and β-sheet structures that previously have been attributed solely to PrP^{Sc}. In particular, ferritin, which is known to consist almost exclusively of α-helices (31) and which we previously identified as the most abundant contaminant in enriched PrP^{Sc} samples (29), absorbed in the α-helix region (1652cm^{-1}) of the spectrum. However, even after many non-PrP proteins were removed and ferritin was reduced by 100 fold, absorbance at 1652cm^{-1} was still detectable. Thus, while contaminating proteins do alter the FTIR spectrum attributed to PrP^{Sc}, the secondary structure remaining after their removal is likely derived from PrP^{Sc} itself suggesting that PrP^{Sc} contains some α-helical, loop, and turn secondary structure.

EXPERIMENTAL PROCEDURES

Reagents and Supplies

Trypsin was purchased from Promega (Madison, WI, USA). Protease inhibitors were from Roche Diagnostics (Indianapolis, IN, USA). Burdick & Jackson brand water and acetonitrile (ACN) were purchased from VWR (Pittsburgh, PA, USA). Formic acid (FA) and Imperial Coomassie blue stain were purchased from Thermo-Fisher Scientific (Pittsburgh, PA, USA). Dithiothreitol, iodoacetamide, tributylphosphine, trifluoroethanol (TFE) and denaturing

buffer (7M urea, 2M thiourea, 1% C_7BzO, 40 mM Tris, pH 10.4) were purchased from Sigma (St. Louis, MO, USA). The PlusOne Silver Staining Kit (GE Healthcare) was used to run SDS-PAGE gels.

Preparation of enriched PrP^{Sc}

Brain homogenates were collected previously as described (29) and enriched PrP^{Sc} samples were prepared by minor modifications to the method of Bolton (21;23). This isolation of PrP^{Sc} includes a series of centrifugation steps, removal of nucleic acids by DNAse and RNAse, and treatment with proteinase K to remove those proteins that are not protease resistant. Each preparation consisted of approximately 100 mL of 10 % weight/volume (w/v) brain homogenate (10 grams of pooled brains). Three independent PrP^{Sc} preparations were derived from hamsters infected with 263K, two from the brains of mice infected with prion strain 79A and one from the brains of mice infected with prion strain 22A. Age-matched control preparations were also done multiple times using either mouse or hamster brains. The 7 – 9 month old C57BL/6 mice were purchased from Jackson Laboratory (Bar Harbor, ME, USA). Syrian golden hamsters were purchased from Harlan Laboratories (USA) and euthanized at approximately 100 days of age for use as age-matched controls. Enriched PrP^{Sc} samples were isolated as pellets, resuspended at a ratio of 50 – 100 μL per gram of starting brain, and stored at 4 °C in 0.5% SB3-14/PBS.

Density Equilibrium Gradients

The components of the enriched PrP^{Sc} pellets were separated by their buoyant densities during sedimentation to equilibrium ultracentrifugation in a sucrose gradient. Sucrose was dissolved in a mixture of deuterated water (D_2O), 10X PBS, and 20% sarkosyl for final concentrations of 1X PBS pH 7.2 and 1% sarkosyl. Polycarbonate tubes for ultracentrifugation were slowly layered with 600 μL 87% w/v sucrose, 800 μL 74% w/v sucrose, 800 μL 53% w/v sucrose, and 400 μL of D_2O/PBS/sarkosyl. Either 110 or 330 μL of enriched PrP^{Sc} pellet was diluted to 440 μL with PBS and Sarkosyl. A portion of each sample (400 μL) was overlaid on the sucrose gradient. After 15 hours at 55,000 rpm (368,000 *g*) in an SW-55 rotor, 200 to 400 μL fractions were collected from the top using 1000 μL pipet tips with the ends cut to a wide bore. Pelleted material was resuspended in 400 μL of PBS/1% sarkosyl and considered the final fraction. For Figures 5 and 6, the terms 263K-Un and 22A-Un are used to denote these preparations prior to fractionation and the fractionated samples are labeled according to the fraction numbers that were used for FTIR analysis.

Western blots

Proteins were separated by SDS-PAGE and transferred to PVDF membrane by wet transfer using Towbin's buffer at 0.3 A for 1 hour. For PrP^{Sc} detection in Figure 1, samples were probed with mouse monoclonal antibody 6D11 (Covance, USA), which recognizes mouse PrP residues 93–109 at a dilution of 1:15,000. The secondary antibody was IRDye 800CW Goat Anti-Mouse (Li-Cor Biosciences, USA) used at a 1:15,000 dilution in TBST buffer as recommended by the manufacturer. An Odyssey imaging system (Li-Cor) using the 800 channel was used to visualize PrP^{Sc} by fluorescent detection and Sharp pre-stained molecular weight markers were detected using the 700 channel.

Sensitive detection of ferritin, shown in the right column of Figure 4, was facilitated by the use of acrylamide gradient gels and the omission of reducing agents in the sample buffer. Samples for ferritin immunoblots were boiled for 10 min in Laemmli sample buffer with 5% SDS, run on Criterion 4 –12% Bis-Tris gels at 150 Volts for 45 min, and then transferred to PVDF membrane at 40 Volts overnight or 100 Volts for one hour. The membrane was blocked with TBST/2% ECL Advance Blocker/Diluent, which was also used as the diluent

for primary and secondary antibodies. Anti-ferritin antibody (Abcam #ab71562) was used at 1:5000, and HRP-labeled anti-rabbit IgG secondary antibody (Santa Cruz #sc-2963) at 1:100,000, each incubated for 1 hour followed by 2 hours of post primary antibody wash in TBST and another 2 hours of wash after the secondary antibody. Blots were developed using the ECL Advance kit. The PVDF membrane used for ferritin western blot was then washed in TBST (not stripped), and re-probed with anti-PrP monoclonal antibody 6D11 at 1:10,000 and anti-mouse IgG at 1:40,000 with ECL detection. The PrP^{Sc} signal was much greater than the ferritin signal and ferritin bands were not observed during the short exposures with the lower sensitivity chemiluminescent reagent used to detect PrP^{Sc}.

Attenuated total reflectance fourier transform infrared spectroscopy (ATR-FTIR or FTIR)

Proteins in 50 μL of crude PrP^{Sc} or control preparations were isolated by centrifugation (Beckman 100.1 rotor, 100,000 rpm, 30 min, 4 °C). Fractions from the sucrose gradients containing the majority of the PrP^{Sc} in the gradient (typically fractions ~4–6, see Figure 4) were diluted two to three-fold in water to reduce their density to a value lower than the PrP^{Sc} particles and then centrifuged (Beckman 100.3 rotor, 100,000 rpm, 2 hours, 4°C). Proteins from gradient fractions identified as high in ferritin (typically fractions 10–13, see Figure 4) were concentrated by dilution and centrifugation as was done for PrP^{Sc} fractions. Pellets were washed in water, resuspended in 50 μL of water, and dried into a thin dehydrated film with a stream of dry nitrogen onto a universal ATR unit with a Diamond/ZnSe surface (Perkin-Elmer). Data were collected with a System 100 FTIR spectrometer equipped with a liquid nitrogen cooled MCT detector in transmittance mode over a 1400–1800 cm^{-1} scan range at 1 cm/sec OPD velocity with 4 cm^{-1} resolution at 1 cm^{-1} data intervals using strong apodization with 64 cumulative scans for each sample. Spectral processing, including background correction for the removal of water vapor and CO_2, were done with Spectrum v6.3.5.0 software (Perkin-Elmer). Primary spectra were translated from percent transmittance to absorbance mode and then used to derive deconvoluted or second derivative spectra.

HPLC-chip based nanospray LC-MS/MS

PrP^{Sc} preparations for LC-MS/MS analysis were subjected to overnight tryptic digestion in a mixture of 10% TFE in 50mM ammonium bicarbonate, pH 8.0 at 37°C as described previously (29). Approximately 190 in-gel digests were analyzed from the 3 replicates of hamster-adapted 263K samples. Likewise, duplicate batches of Coomassie blue-stained bands from each of the mouse samples were overnight digested for LC/MS/MS analysis. Peptides were identified by LC-MS/MS using an Agilent 1200 connected to an XCT Ultra Ion Trap via a microfluidic HPLC chip interface and a nanospray source using the same instrument parameters as described previously (29).

Mass spectrometry data processing and analysis

Raw data were processed into peak lists and then exported as MGF files using the Ion Trap data analysis software, version 3.4, Rev 6.2 supplied by Agilent Technologies. Peak lists from the mouse samples were searched using MASCOT Daemon (32) against an Sprot fasta-formatted database with 16,315 mouse-specific sequences. A parent ion mass tolerance of 2.2 Da was used with a 1.0 monoisotopic fragment ion mass tolerance in separate trypsin and then semi-trypsin search modes. Cysteine was assigned a static modification mass of +57 Da and methionine had a variable modification mass of +16 Da. The same MGF files were then searched against a separate decoy database composed of reversed sequences. Peptides had to be consistent with tryptic or semi-tryptic cleavage fragmentation patterns in order to be considered valid. The DAT files generated by MASCOT were refined to a ≤1 % protein false discovery rate (FDR) based upon the PROVALT algorithm (33) as implemented by the proteomics software suite ProteoIQ (NuSep, Inc Athens, GA, USA).

Both tryptic and semi-tryptic searches were clustered against the subset database of 1% protein FDR obtained from the tryptic peptides. Thus, no new protein identifications could be introduced with the semi-trypsin input files. This process maintained the rigor of the 1% protein FDR validity threshold while expanding sequence coverage to include semi-tryptic peptides; a necessity dictated by the fact that the PrP^{Sc} preparations include proteinase K treatment prior to denaturation and in-gel tryptic digestion. The data were then further filtered to exclude keratin sequences and to include only proteins that were identified by at least 2 peptides having distinct m/z values and ≥7 amino acids in length. The final protein mouse-associated PrP^{Sc} protein lists are shown in Table 1 and a complete list of peptides is provided as supplementary data.

While the Syrian hamster (*Mesocricetus auratus*) genome was not publically available at the time of our study, we had access to some partial hamster genome sequence data derived from mRNA samples (unpublished data), the details of which will be described elsewhere. In the case of ferritin and apolipoprotein E (apoE), the hamster-specific sequences provided better sequence coverage and a greater number of spectral counts than the publically available sequences. However, with the exception of ferritin and apoE, we found that the data could be more efficiently searched using publically available sequences. Thus, the LC-MS/MS data from the hamster samples was searched using a custom database composed of *rodentia* sequences (www.uniprot.org) in which entries for PrP, apoE, and ferritin were replaced with hamster-specific sequences. The final database, with 25,527 sequences, was reversed with a PERL script for decoy searches and searched using the same parameters as described above. Protein identifications were limited to a FDR of ≤1% including trypsin and semi-trypsin peptides as described above and then further filtered to include only proteins that were identified by at least 3 peptides with unique m/z values. Keratin was also filtered from the list. The identified scrapie-associated proteins are listed in Table 2 from highest to lowest in terms of relative spectral counts. A complete list of peptides is provided as supplementary material.

RESULTS

Enrichment of PrP^{Sc}

Enriched PrP^{Sc} isolated from scrapie-infected tissues has a high titer of infectivity as measured in laboratory animals (22;34) and retains its ability to encode strain-specific phenotypes such as patterns of PrP^{Sc} deposition and histopathological lesion profiles (S. Priola, unpublished data). Three well-characterized rodent-adapted TSE agents with distinct pathologies were selected for this study. Mouse strains 79A and 22A (35;36) originated from sheep scrapie and 79A was derived by further passage through a goat line and then cloned by serial passage using the minimum infectious dose in C57BL/6 mice (37). The Syrian golden hamster-adapted 263K strain displays exceptionally high infectivity titers and short incubation times in clinically affected hamsters (38).

Initial enrichments of PrP^{Sc} from infected brains prior to fractionation were done as described in the methods section. Each of those samples was subjected to SDS-PAGE followed by silver staining, Coomassie blue staining and immunoblotting with anti-PrP mouse monoclonal antibody 6D11 (Figure 1). The Coomassie blue and silver stains of the preparations from uninfected brain material (mock) displayed prominent banding at approximately 20 kDa in addition to some minor bands at different molecular weights. However, only infected samples displayed the characteristic PrP^{Sc} pattern at approximately 20–32 kDa. The 6D11 immunoblot confirmed that protease resistant PrP^{Sc} was present only in those samples isolated from infected animals (Figure 1, C–D).

Structural analysis of enriched PrP^{Sc}

For the structural analysis of PrP^{Sc}, we used attenuated total reflectance fourier transform infrared spectroscopy (39) (ATR-FTIR, here used synonymously with FTIR), whereby aggregated material was dried as a thin film upon a Diamond/ZnSe reflective surface. The second derivative FTIR spectra of PrP^{Sc} derived from strains 22A, 79A and 263K are shown in Figure 2 above the corresponding spectra derived from age-matched uninfected animals. Each of the PrP^{Sc} samples displayed reproducibly distinctive β-sheet banding patterns at 1621–1636cm^{-1} as well as some additional, less prominent banding at ~1650–1670cm^{-1}. The 1650–1670cm^{-1} region of the spectrum has been associated with multiple secondary structure assignments, including α-helix, β-turn, loops as well as random coil (40–44). Representative FTIR spectra for 263K-PrP^{Sc} from our preparations (see Figure 2) are consistent with previously published data, displaying a characteristic banding pattern at 1624 and 1636cm^{-1} that has been interpreted as β-sheet (5;6). Mouse-derived 79A-PrP^{Sc} displayed significant β-sheet character with distinctive peaks at 1620, 1626, and 1632cm^{-1}, while 22A-PrP^{Sc} shows similar banding at only 1620 and 1632cm^{-1} (Figure 2). Thus, although each PrP^{Sc} mixture is composed mostly of β-sheet character in addition to a less prominent distribution of bands at ~ 1650–1670cm^{-1} (Table S1), distinctive spectra were observed for each strain. When compared to PrP^{Sc}, the uninfected mock samples from both mouse and hamster brains also displayed significant protein secondary structure, although with higher ratios of apparent α-helix to β-sheet character (Figure 2) in addition to strong β-sheet banding centered at 1630cm^{-1} which differed from the PrP^{Sc}-associated spectra.

Protein profiling

The fact that we detected α-helix, turn and loop structure in addition to significant β-sheet character in our mock samples suggested that some non-PrP proteins could potentially complicate the FTIR analysis in our infectious preparations. In order to identify what non-PrP^{Sc} proteins might contribute to the observed banding in our FTIR spectra, we profiled our samples by nanospray LC-MS/MS. Protein identifications specific to mouse 79A and 22A preparations are shown in Table 1 while hamster-specific identifications are shown in Table 2, listed from highest to lowest in terms of the number of assigned MS/MS spectra (spectral counts) found in a sample. Semi-quantitative estimates of relative apparent abundance between key proteins within sample sets were made based upon the established positive correlation between protein concentration and the number of spectral counts in a sample (45). Ferritin heavy and light subunits were the single most abundant impurity in all of the PrP^{Sc} samples (Tables 1 and 2, Figure 3A) and ferritin was the most prominent protein contaminant in the mock preparations (Table 3 and Figure 3B). Various ribosomal subunits, when combined, were also quite abundant in the mock hamster preparations (Figure 3B and Table 3), although this was not the case with mock mouse samples (Table 3). Proteins with low relative abundance were quite variable between strains while proteins typically found in higher amounts such as ferritin, apolipoprotein E (apoE), and myelin proteolipid protein were found in all of the PrP^{Sc} samples (Figure 3C). Consistent with previous reports by us and others (28;29), apoE was always a significant component of the infected samples but as yet has not been found in our mock preparations (Tables 1–3 and reference (29)).

Buoyant density gradient separation of PrP^{Sc} from other proteins

The FTIR spectra from the mock samples contained a high degree of α-helical character, likely due to the presence of ferritin (Table 3), which is composed almost exclusively of α -helical bundles (31). Given that ferritin was the most abundant contaminant in the PrP^{Sc} samples, we were concerned that ferritin might interfere with the interpretation of the PrP^{Sc} FTIR spectra, especially in the α-helix region of the spectrum. We therefore developed a method to separate PrP^{Sc} from ferritin and potentially other contaminants in order to further

analyze the individual components by FTIR. Purified PrP^{Sc} samples from mouse 79A, 22A and hamster 263K-derived material were subjected to sucrose equilibrium gradients resulting in thirteen fractions from each of the original samples (Figure 4A–F). Corresponding material from the uninfected mock purifications was fractionated by the same treatment (Figure 4G–H). In all samples, the bulk of the ferritin was found in the lowest fractions corresponding to the highest sucrose concentrations or in the pellet itself (Figure 4, right panels), consistent with the unusually high density of iron-loaded ferritin. We found that for 22A and 263K-PrP^{Sc} samples, the ferritin was reduced by approximately 100-fold relative to the amount of PrP^{Sc} recovered with this treatment (Supplemental Figure 1).

Structural analysis of fractionated PrP^{Sc} and non-PrP^{Sc} proteins

After subjecting our samples to density gradient fractionation, we were able to make a comparison of the PrP^{Sc} spectra before and after removal of the major contaminants. In the case of hamster-derived 263K, the removal of ferritin revealed increases in banding at 1652cm^{-1}, 1668cm^{-1} (Figure 5, 263K-F5–6), and in the β-sheet region spanning ~1605–1640 (Table S1) in the PrP^{Sc} fractions (Figure 4E and F). Consistent with the known structure of ferritin (31), the ferritin-containing fractions extracted from purified hamster 263K-PrP^{Sc} (Figure 4F, fractions 11–13) displayed predominant banding in the α-helical region (~1652cm^{-1}) of the FTIR spectrum (Figure 5, 263K-F11–13). Control samples of commercial ferritin also display strong banding at 1652cm^{-1} (Supplemental Figure 2), consistent with the presence of α-helix. Thus, the removal of ferritin and other proteins altered the observed banding from approximately 1650 – 1670cm^{-1} of the 263K-PrP^{Sc} FTIR spectrum.

Although we were unable to recover enough PrP^{Sc} from the gradient fractionations to thoroughly analyze mouse 79A-PrP^{Sc} (data not shown), sufficient PrP^{Sc} was recovered from the mouse 22A-PrP^{Sc} gradient fractionations. FTIR analysis of fractionated versus unfractionated mouse 22A-PrP^{Sc}, termed 22A-Un in Figure 6, revealed a decrease in apparent α-helical banding at approximately 1652cm^{-1} (Figure 6B, compare F4–6 to F10–13) following the removal of ferritin and other non-PrP components (Figure 4, C–D). Similar to 263K-PrP^{Sc}, we also observed an increase in the relative proportion of β-sheet peak area from ~1605–1640 (Table S1). The bottom fractions in the density gradient (Figure 4D, fractions 10–13) were examined by western blot and mass spectrometry and revealed that this material was composed almost entirely of ferritin while the FTIR spectra of those fractions displayed significant α-helical banding at ~1652–1655cm^{-1} (Figure 6B, 22A-F10–13). The relatively high abundance of ferritin in the unfractionated 22A preparation, (termed Un in Figure 6A) coupled with its high α-helical content (Figure 6B, F10–13) suggests that the loss of α-helical structure in fractionated 22A-PrP^{Sc} (22A-F4–6) is due to the removal of ferritin. Thus, in the case of 22A-PrP^{Sc}, where the contaminants were relatively abundant (see Table 1 and Figure 6A), it was easier to detect an effect upon the FTIR spectrum when most of the contaminants were removed. However, in the case of 263K-PrP^{Sc}, where the relative contaminant abundances prior to fractionation were relatively low, changes in the FTIR spectra could be detected but the changes were not as prominent in terms of the relative amount of peak area affected.

DISCUSSION

While it is known that PrP^{Sc} contains a much higher degree of β-sheet character than does PrP^{C}, whether or not it contains a significant amount of α-helical character is less clear. Some reports have suggested that PrP^{Sc} retains a portion of its original α-helix (6;14;15;46), yet it has also been reported that PrP^{Sc} is devoid of α-helical character (13;16;17). Following removal of ferritin from hamster 263K-PrP^{Sc}, our spectra nonetheless show

absorbance at 1652cm^{-1}, suggesting that this absorbance had been previously masked by non-PrP proteins. Thus, increasing the sample purity by adding the extra step of density gradient separation enabled the detection of this relatively minor absorbance at 1652cm^{-1}. Given the increased purity of the 263K-PrP^{Sc} sample, our results suggest that absorbance in this region is due to PrP^{Sc} itself and are consistent with the conclusion that hamster 263K-PrP^{Sc} has some α-helical, loop, or turn structure.

Removal of non-PrP protein contaminants, including a 100-fold reduction in ferritin, had the opposite effect on the FTIR spectrum assigned to mouse 22A-PrP^{Sc}. In the case of 22A-PrP^{Sc}, removal of the contaminants led to a noticeable decrease in absorbance in the 1652cm^{-1} region of the spectrum. There was also a narrowing in a β-sheet banding (~1628cm^{-1}) in fractionated versus unfractionated 22A-PrP^{Sc}. However, there was an overall increase in the proportion of β-sheet relative to total peak area in the spectrum (Table S1). Based upon the semi-quantitative technique of spectral counting (45), the relative abundance of ferritin in the mouse 22A-PrP^{Sc} preparations was 3-fold higher than in the hamster 263K-PrP^{Sc} samples while the amount of PrP^{Sc} was lower. Thus, in the 22A-PrP^{Sc} sample, ferritin is likely present in amounts sufficient for the detection of its secondary structure by FTIR. Ferritin is a protein with significant α-helical content (31) that strongly absorbs in the 1652cm^{-1} region of the FTIR spectrum (Supplementary Figure 2). Since the changes at 1652cm^{-1} and 1628cm^{-1} in the FTIR spectrum assigned to 22A-PrP^{Sc} were precisely where major absorbances were centered in the ferritin-containing gradient fractions (Figure 6), our data strongly suggest that at least some of the absorbance in these regions was derived from ferritin. Overall, our analysis of both 263K and 22A-PrP^{Sc} suggests that PrP^{Sc} may maintain some of the α-helical, loop, and turn content of PrP^{C} although the relative amounts may vary between prion strains.

Mock PrP^{Sc} purifications also yield proteins based upon their tendency to aggregate and resist proteolytic digestion and they often contain many of the same non-PrP proteins that are found in the corresponding prion-infected samples (*e.g*, Table 3). When compared to infectious PrP^{Sc}, mock samples absorb proportionally more in the α-helix/turn/loop region (~1650 – 1670cm^{-1}) (43) than in the β-sheet region of the spectrum. The mock spectra, however, did display distinct banding at ~1630cm^{-1} indicating that proteins with β-sheet are present. As with the PrP^{Sc} samples, a portion of the absorbance in the α-helical 1652cm^{-1} region of the FTIR spectrum likely comes from ferritin. It is less clear what other proteins in the mock PrP^{Sc} samples might be responsible for β-sheet banding from ~1620–1636 cm^{-1}. However, the non-ferritin proteins shown in Table 3 provide key candidates due to their protease-resistance and propensity to aggregate.

Other than ferritin and PrP^{Sc}, the only other protein that we have consistently identified in samples enriched for PrP^{Sc} is apoE. Using tandem mass spectroscopy, we have found apoE in multiple PrP^{Sc} samples derived from five different prion strains (three in the current study and two in (29)) but have not found it in multiple samples from three independent mock preparations (two in the current study and three in (29)). Genomic analysis has shown that the apoE gene is upregulated in prion and other amyloid diseases (47–50) and has been found in biomarker studies related to prion disease (51;52). ApoE transports cholesterol in plasma and in the brain, a critical function known to be perturbed in many neurodegenerative disorders including Alzheimer's disease (53). ApoE is also known to bind various amyloidogenic proteins (54) and has been shown to co-localize with PrP^{Sc} deposits in vivo (28;55). Thus, its presence in PrP^{Sc} preparations from prion-infected brains may simply be due to its ability to bind PrP^{Sc}. However, it should be noted that since increased levels of apoE appear to be specifically associated with prion infected brain material, it is possible that this protein plays a role in prion disease pathogenesis.

Our data demonstrate the importance of considering the potentially confounding effects of co-purifying proteins on the structural analysis of PrP^{Sc}. In addition, the presence of significant levels of ferritin and apoE in PrP^{Sc} preparations that have been profiled by tandem mass spectrometry (28;29) underscores the potential difficulties in interpreting data which rely on purified PrP^{Sc} to study various aspects of prion biology such as prion uptake and trafficking. We have found that the simple addition of a density equilibrium gradient to a PrP^{Sc} purification that is based upon repeated centrifugation and proteinase K treatment can enhance the purity of PrP^{Sc}. Addition of such a step is strongly recommended for any study that requires purified PrP^{Sc}.

Supplementary Material

Refer to Web version on PubMed Central for supplementary material.

Acknowledgments

The authors would like to thank Drs. Bruce Chesebro, Gerald Baron, and Byron Caughey for critically evaluating the manuscript. Anita Mora and Austin Althman provided technical assistance in preparation of the figures. The authors thank Craig Martens, Kimmo Virtaneva and Steve Porcella from the Rocky Mountain Research Technologies Branch for the extraction of tissue used for obtaining hamster DNA sequencing data. The authors also thank Brent Weatherly from NuSep, Inc for helpful discussions with ProteoIQ software.

Funding Sources. This research was supported by intramural research program of the National Institute of Allergy & Infectious Disease, National Institutes of Health (Project #1-Z01-AI000752-12). PAW was supported by National Institutes of Health grant EY007755.

Abbreviations

LC-MS/MS	liquid chromatography tandem mass spectrometry
TSE	Transmissible Spongiform Encephalopathy
ATR-FTIR	attenuated total reflectance fourier transform infrared spectroscopy
FTIR	fourier transform infrared spectroscopy

References

1. Chesebro B. Introduction to the transmissible spongiform encephalopathies or prion diseases. Br. Med. Bull. 2003; 66:1–20. [PubMed: 14522845]
2. Moore RA, Taubner LM, Priola SA. Prion protein misfolding and disease. Curr. Opin. Struct. Biol. 2009; 19:14–22. [PubMed: 19157856]
3. Safar J, Wille H, Itri V, Groth D, Serban H, Torchia M, Cohen FE, Prusiner SB. Eight prion strains have PrP(Sc) molecules with different conformations. Nat. Med. 1998; 4:1157–1165. [PubMed: 9771749]
4. Thomzig A, Spassov S, Friedrich M, Naumann D, Beekes M. Discriminating scrapie and bovine spongiform encephalopathy isolates by infrared spectroscopy of pathological prion protein. J. Biol. Chem. 2004; 279:33847–33854. [PubMed: 15155741]
5. Spassov S, Beekes M, Naumann D. Structural differences between TSEs strains investigated by FT-IR spectroscopy. Biochim. Biophys. Acta. 2006; 1760:1138–1149. [PubMed: 16730908]
6. Caughey B, Raymond GJ, Bessen RA. Strain-dependent differences in beta-sheet conformations of abnormal prion protein. J. Biol. Chem. 1998; 273:32230–32235. [PubMed: 9822701]
7. Wiltzius JJ, Landau M, Nelson R, Sawaya MR, Apostol MI, Goldschmidt L, Soriaga AB, Cascio D, Rajashankar K, Eisenberg D. Molecular mechanisms for protein-encoded inheritance. Nat. Struct. Mol. Biol. 2009; 16:973–978. [PubMed: 19684598]
8. Caughey B, Baron GS, Chesebro B, Jeffrey M. Getting a grip on prions: oligomers, amyloids, and pathological membrane interactions. Annu. Rev. Biochem. 2009; 78:177–204. [PubMed: 19231987]

9. Riek R, Hornemann S, Wider G, Billeter M, Glockshuber R, Wuthrich K. NMR structure of the mouse prion protein domain PrP(121–231). Nature. 1996; 382:180–182. [PubMed: 8700211]
10. Zahn R, Liu A, Luhrs T, Riek R, von Schroetter C, Garcia FL, Billeter M, Calzolai L, Wider G, Wuthrich K. NMR solution structure of human prion protein. Proc. Natl. Acad. Sci. USA. 2000; 97:145–150. [PubMed: 10618385]
11. Lysek DA, Schorn C, Nivon LG, Esteve-Moya V, Christen B, Calzolai L, von SC, Fiorito F, Herrmann T, Guntert P, Wuthrich K. Prion protein NMR structures of cats, dogs, pigs, and sheep. Proc. Natl. Acad. Sci. U. S. A. 2005; 102:640–645. [PubMed: 15647367]
12. Knaus KJ, Morillas M, Swietnicki W, Malone M, Surewicz WK, Yee VC. Crystal structure of the human prion protein reveals a mechanism for oligomerization. Nat. Struct. Biol. 2001; 8:770–774. [PubMed: 11524679]
13. Safar J, Roller PP, Gajdusek DC, Gibbs CJ Jr. Conformational transitions, dissociation, and unfolding of scrapie amyloid (prion) protein. J. Biol. Chemy. 1993; 268:20276–20284.
14. Caughey BW, Dong A, Bhat KS, Ernst D, Hayes SF, Caughey WS. Secondary Structure-Analysis of the Scrapie-Associated Protein Prp 27–30 in Water by Infrared-Spectroscopy. Biochemistry. 1991; 30:7672–7680. [PubMed: 1678278]
15. Pan K-M, Baldwin M, Nguyen J, Gasset M, Serban A, Groth D, Mehlhorn I, Huang Z, Fletterick RJ, Cohen FE, Prusiner SB. Conversion of alpha-helices into beta-sheets features in the formation of the scrapie prion protein. Proc. Natl. Acad. Sci. USA. 1993; 90:10962–10966. [PubMed: 7902575]
16. Baron GS, Hughson AG, Raymond GJ, Offerdahl DK, Barton KA, Raymond LD, Dorward DW, Caughey B. Effect of glycans and the glycophosphatidylinositol anchor on strain dependent conformations of scrapie prion protein: improved purifications and infrared spectra. Biochemistry. 2011; 50:4479–4490. [PubMed: 21539311]
17. Smirnovas V, Baron GS, Offerdahl DK, Raymond GJ, Caughey B, Surewicz WK. Structural organization of brain-derived mammalian prions examined by hydrogen-deuterium exchange. Nat. Struct. Mol. Biol. 2011; 18:504–506. [PubMed: 21441913]
18. Demarco ML, Silveira J, Caughey B, Daggett V. Structural Properties of Prion Protein Protofibrils and Fibrils: An Experimental Assessment of Atomic Models. Biochemistry. 2006; 45:15573–15582. [PubMed: 17176078]
19. Govaerts C, Wille H, Prusiner SB, Cohen FE. Evidence for assembly of prions with left-handed beta-helices into trimers. Proc Natl Acad Sci U. S. A. 2004; 101:8342–8347. [PubMed: 15155909]
20. Diringer H, Hilmert H, Simon D, Werner E, Ehlers B. Towards purification of the scrapie agent. Eur. J. Biochem. 1983; 134:555–560. [PubMed: 6411468]
21. Bolton DC, McKinley MP, Prusiner SB. Identification of a protein that purifies with the scrapie prion. Science. 1982; 218:1309–1311. [PubMed: 6815801]
22. Gabizon R, McKinley MP, Groth D, Prusiner SB. Immunoaffinity purification and neutralization of scrapie prion infectivity. Proc. Natl. Acad. Sci. USA. 1988; 85:6617–6621. [PubMed: 3137571]
23. Raymond, GJ.; Chabry, J. Purification of the pathological isoform of prion protein (PrPSc or PrPres) from transmissible spongiform encephalopathy-affected brain tissue. In: Lehmann, S.; Grassi, J., editors. Techniques in Prion Research. Birkhauser Verlag; Basel: 2004. p. 16-26.
24. Prusiner SB, Bolton DC, Groth DF, Bowman KA, Cochran SP, McKinley MP. Further purification and characterization of scrapie prions. Biochemistry. 1982; 21:6942–6950. [PubMed: 6818988]
25. Appel TR, Dumpitak C, Matthiesen U, Riesner D. Prion rods contain an inert polysaccharide scaffold. Biol. Chem. 1999; 380:1295–1306. [PubMed: 10614822]
26. Stahl N, Borchelt DR, Hsiao K, Prusiner SB. Scrapie prion protein contains a phosphatidylinositol glycolipid. Cell. 1987; 51:229–240. [PubMed: 2444340]
27. Diringer H, Beekes M, Ozel M, Simon D, Queck I, Cardone F, Pocchiari M, Ironside JW. Highly infectious purified preparations of disease-specific amyloid of transmissible spongiform encephalopathies are not devoid of nucleic acids of viral size. Intervirology. 1997; 40:238–246. [PubMed: 9612725]
28. Giorgi A, Di FL, Principe S, Mignogna G, Sennels L, Mancone C, Alonzi T, Sbriccoli M, De PA, Rappsilber J, Cardone F, Pocchiari M, Maras B, Schinina ME. Proteomic profiling of PrP27–30-

enriched preparations extracted from the brain of hamsters with experimental scrapie. Proteomics. 2009; 9:3802–3814. [PubMed: 19637240]

29. Moore RA, Timmes A, Wilmarth PA, Priola SA. Comparative profiling of highly enriched 22L and Chandler mouse scrapie prion protein preparations. Proteomics. 2010; 10:2858–2869. [PubMed: 20518029]
30. Wadsworth JD, Hill AF, Joiner S, Jackson GS, Clarke AR, Collinge J. Strain-specific prion-protein conformation determined by metal ions. Nat. Cell Biol. 1999; 1:55–59. [PubMed: 10559865]
31. Crichton RR, Declercq JP. X-ray structures of ferritins and related proteins. Biochim. Biophys. Acta. 2010; 1800:706–718. [PubMed: 20363295]
32. Perkins DN, Pappin DJ, Creasy DM, Cottrell JS. Probability-based protein identification by searching sequence databases using mass spectrometry data. Electrophoresis. 1999; 20:3551–3567. [PubMed: 10612281]
33. Weatherly DB, Atwood JA III, Minning TA, Cavola C, Tarleton RL, Orlando R. A Heuristic method for assigning a false-discovery rate for protein identifications from Mascot database search results. Mol. Cell Proteomics. 2005; 4:762–772. [PubMed: 15703444]
34. Silveira JR, Raymond GJ, Hughson AG, Race RE, Sim VL, Hayes SF, Caughey B. The most infectious prion protein particles. Nature. 2005; 437:257–261. [PubMed: 16148934]
35. Bruce ME. Scrapie strain variation and mutation. Br. Med. Bull. 1993; 49:822–838. [PubMed: 8137131]
36. Cunningham C, Deacon RM, Chan K, Boche D, Rawlins JN, Perry VH. Neuropathologically distinct prion strains give rise to similar temporal profiles of behavioral deficits. Neurobiol. Dis. 2005; 18:258–269. [PubMed: 15686954]
37. Bruce ME, McConnell I, Fraser H, Dickinson AG. The disease characteristics of different strains of scrapie in Sinc congenic mouse lines: implications for the nature of the agent and host control of pathogenesis. J. Gen. Virol. 1991; 72:595–603. [PubMed: 1672371]
38. Kimberlin RH, Walker CA, Fraser H. The genomic identity of different strains of mouse scrapie is expressed in hamsters and preserved on reisolation in mice. J. Gen. Virol. 1989; 70:2017–2025. [PubMed: 2504883]
39. Seshadri S, Khurana R, Fink AL. Fourier transform infrared spectroscopy in analysis of protein deposits. Methods Enzymol. 1999; 309:559–576. [PubMed: 10507048]
40. Haris PI. Can infrared spectroscopy provide information on protein-protein interactions? Biochem. Soc. Trans. 2010; 38:940–946. [PubMed: 20658981]
41. Surewicz WK, Mantsch HH, Chapman D. Determination of protein secondary structure by Fourier transform infrared spectroscopy: a critical assessment. Biochemistry. 1993; 32:389–394. [PubMed: 8422346]
42. Wilder CL, Friedrich AD, Potts RO, Daumy GO, Francoeur ML. Secondary structural analysis of two recombinant murine proteins, interleukins 1 alpha and 1 beta: is infrared spectroscopy sufficient to assign structure? Biochemistry. 1992; 31:27–31. [PubMed: 1731876]
43. Barth A. Infrared spectroscopy of proteins. Biochimica et Biophysica Acta-Bioenergetics. 2007; 1767:1073–1101.
44. Susi H, Byler DM. Protein structure by Fourier transform infrared spectroscopy: second derivative spectra. Biochem. Biophys. Res. Commun. 1983; 115:391–397. [PubMed: 6615537]
45. Lundgren DH, Hwang SI, Wu L, Han DK. Role of spectral counting in quantitative proteomics. Expert. Rev. Proteomics. 2010; 7:39–53. [PubMed: 20121475]
46. Gasset M, Baldwin MA, Fletterick RJ, Prusiner SB. Perturbation of the secondary structure of the scrapie prion protein under conditions that alter infectivity. Proc. Natl. Acad. Sci. USA. 1993; 90:1–5. [PubMed: 8419912]
47. Huzarewich RL, Siemens CG, Booth SA. Application of “omics” to prion biomarker discovery. J. Biomed. Biotechnol. 2010; 2010:613504. [PubMed: 20224650]
48. Skinner PJ, Abbassi H, Chesebro B, Race RE, Reilly C, Haase AT. Gene expression alterations in brains of mice infected with three strains of scrapie. BMC. Genomics. 2006; 7:114. [PubMed: 16700923]

49. Sorensen G, Medina S, Parchaliuk D, Phillipson C, Robertson C, Booth SA. Comprehensive transcriptional profiling of prion infection in mouse models reveals networks of responsive genes. BMC. Genomics. 2008; 9:114. [PubMed: 18315872]
50. Twine NA, Janitz K, Wilkins MR, Janitz M. Whole transcriptome sequencing reveals gene expression and splicing differences in brain regions affected by Alzheimer's disease. PLoS. ONE. 2011; 6:e16266. [PubMed: 21283692]
51. Choe LH, Green A, Knight RS, Thompson EJ, Lee KH. Apolipoprotein E and other cerebrospinal fluid proteins differentiate ante mortem variant Creutzfeldt-Jakob disease from ante mortem sporadic Creutzfeldt-Jakob disease. Electrophoresis. 2002; 23:2242–2246. [PubMed: 12210228]
52. Hochstrasser DF, Frutiger S, Wilkins MR, Hughes G, Sanchez JC. Elevation of apolipoprotein E in the CSF of cattle affected by BSE. FEBS Lett. 1997; 416:161–163. [PubMed: 9369204]
53. Kim J, Basak JM, Holtzman DM. The role of apolipoprotein E in Alzheimer's disease. Neuron. 2009; 63:287–303. [PubMed: 19679070]
54. Baumann MH, Kallijarvi J, Lankinen H, Soto C, Haltia M. Apolipoprotein E includes a binding site which is recognized by several amyloidogenic polypeptides. Biochem. J. 2000; 349:77–84. [PubMed: 10861213]
55. Nakamura S, Ono F, Hamano M, Odagiri K, Kubo M, Komatsuzaki K, Terao K, Shinagawa M, Takahashi K, Yoshikawa Y. Immunohistochemical detection of apolipoprotein E within prion-associated lesions in squirrel monkey brains. Acta Neuropathol. 2000; 100:365–370. [PubMed: 10985693]

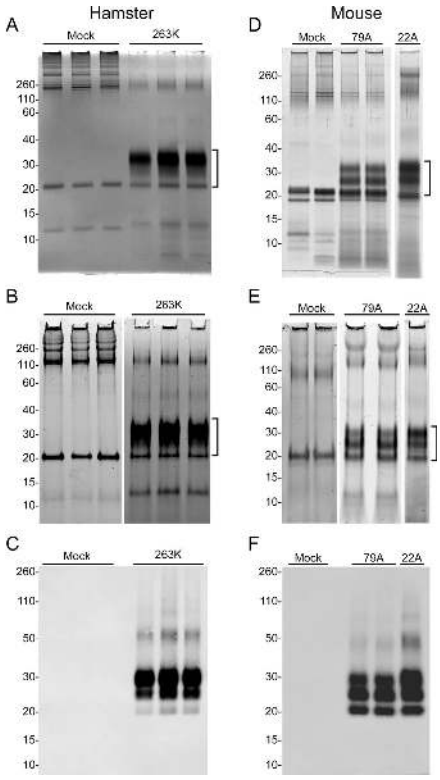

Figure 1. Purification and characterization of mouse and hamster-adapted PrP^{Sc}

Panels on the left represent PrP^{Sc} purified from 263K-infected hamster brain material while those on the right represent PrP^{Sc} purified from the brains of mice infected with the scrapie strains 79A and 22A. Mock represents uninfected brain material from age matched hamsters and mice processed in the same way as the infected brain material. A and D) GE silver stain; B and E) Coomassie blue Imperial stain; C and F) Western blot developed with the anti-PrP mouse monoclonal antibody 6D11. The brackets indicate PrP^{Sc}-specific banding patterns. Molecular mass markers are shown on the left side of each panel. White spaces between lanes in panels B, D and E indicate that the samples were run on separate gels.

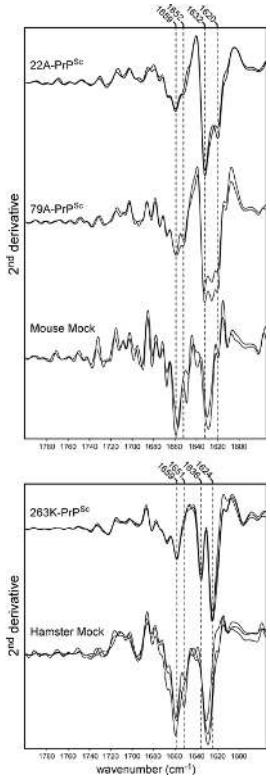

Figure 2. Secondary derivative FTIR spectra of enriched purified PrP^{Sc} prior to fractionation

Purified PrP^{Sc} from scrapie-infected mice and hamsters was compared to similar preparations from uninfected, age-matched controls (mock). Top) Purified PrP^{Sc} from 79A and 22A infected mice versus analogous material from age-matched uninfected mice. Bottom) Purified PrP^{Sc} from 263K infected hamsters versus uninfected, age-matched controls. Specific banding in the α-helical/loop/turn region (~1650–1660cm^{-1}) and the β-sheet region (~1610–1636cm^{-1}) of the spectra are indicated by the dashed vertical lines.

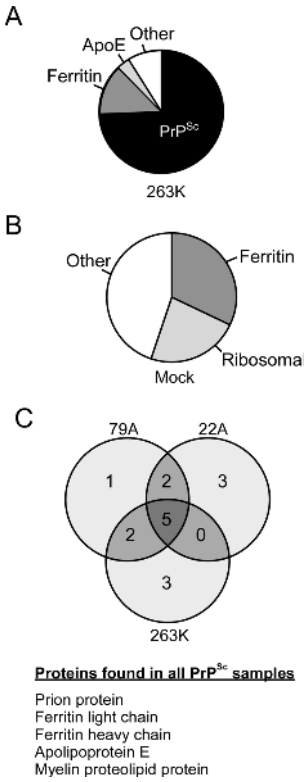

Figure 3. Protein identifications in PrP^{Sc} isolated from different mouse and hamster prion strains

A) Comparison of PrP^{Sc} versus non-PrP^{Sc} proteins in purified hamster 263K-PrP^{Sc}. Relative apparent abundance was based upon the number of assigned MS/MS spectra (*i.e.*, spectral counts). PrP^{Sc} identifications made up 74 % of the total protein identifications in hamster 263K-PrP^{Sc} compared to 13 % from ferritin. The results are tallied cumulatively from 3 independent preparations and 191 LC/MS/MS injections. B) Relative apparent abundance of ferritin versus non-ferritin proteins in hamster mock preparations was based upon the number of assigned MS/MS spectra. Ferritin identifications made up 32 % of the total protein identifications while 23% and 45% were from ribosomal and other proteins, respectively. C) Comparison of protein identifications between PrP^{Sc} from all three strains profiled. The 5 proteins in the Venn diagram that were found in all PrP^{Sc} samples are listed below.

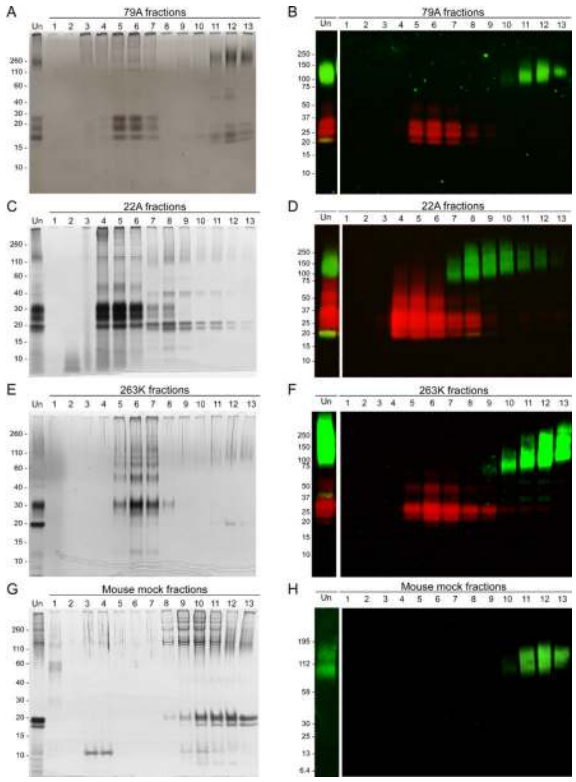

Figure 4. Separation of PrP^{Sc} from ferritin by sucrose equilibrium gradients

A and B) 79A PrP^{Sc}, C and D) 22A-PrP^{Sc}, E and F) 263K-PrP^{Sc} and, G and H) Mouse mock material. The left column panels represent silver stained samples. The first lane of each gel shows unfractionated PrP^{Sc} while the remaining lanes represent the 13 sucrose equilibrium gradient fractions (lanes labeled 1-13). The right column panels represent immunoblots transferred from gradient gels of the same fractions probed successively with anti-ferritin and anti-PrP antibodies. The first lane of each gel shows unfractionated PrP^{Sc} (Un) while the remaining lanes represent the 13 sucrose equilibrium gradient fractions (lanes labeled 1-13). Red represents PrP^{Sc} and green represents ferritin. The yellow signal in the first lane of unfractionated material indicates regions in the lane where PrP^{Sc} and ferritin overlap. Molecular mass markers (kDa) are indicated on the left of each panel.

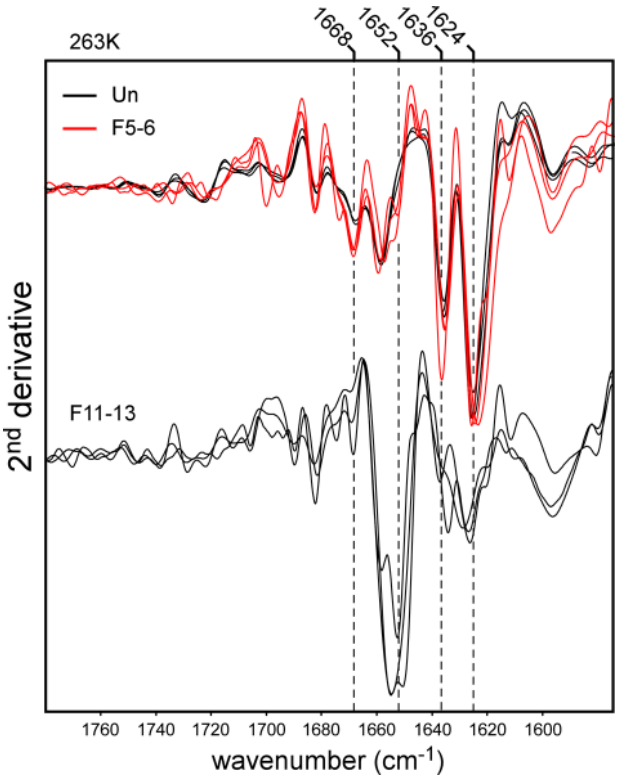

Figure 5. Minimal alteration of secondary structure in fractionated versus unfractionated 263K-PrP^{Sc}

Black lines in the upper portion of the panel represent secondary derivative FTIR spectra of enriched PrP^{Sc} from three independent preparations prior to sucrose fractionation (263K-Un). The red lines represent secondary derivative FTIR spectra of hamster PrP^{Sc} fractionated through a sucrose gradient (263K-F5–6). The fractionated spectra (F5–6) display minor additional banding at 1652cm^{-1} when compared to the unfractionated sample (Un). PrP^{Sc} is a higher percentage of total protein in 263K-F5–6 than in 263K-Un. The lower portion of the panel shows the ferritin-containing fractions (263K-F11–13) with major banding in the α-helical/loop region (centered at 1652cm^{-1}) and minor banding in the β-sheet region (~1620–1638cm^{-1}) as indicated by the dashed vertical lines.

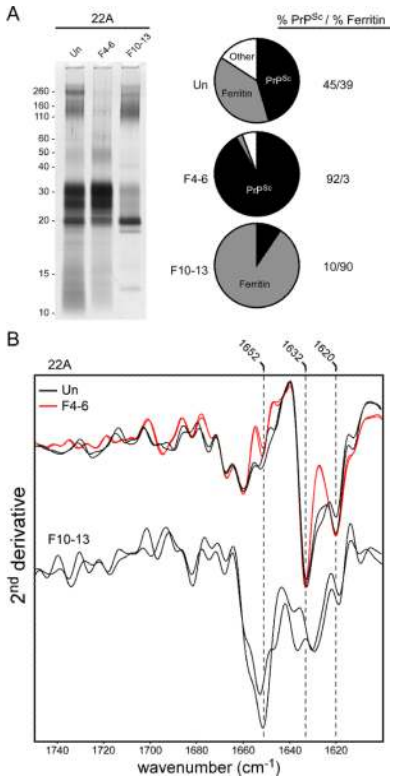

Figure 6. Removal of ferritin decreases α-helical structure in 22A-PrP^{Sc} spectra

A) Silver stained gel comparing unfractionated 22A-PrP^{Sc} (Un), fractionated PrP^{Sc} (F4–6) and fractionated ferritin-enriched fractions (22A-F10–13). The relative apparent abundances of PrP^{Sc} versus ferritin in each sample are based upon the ratio of the number of assigned spectra for each and percentages are shown to the right. The majority of the protein in fraction 22A-F4–6 is PrP^{Sc} while the majority of the protein in 22A-F10–13 is ferritin. B) Overlay of duplicate secondary derivative FTIR spectra from the unfractionated 22A-Un (black lines) and fractionated PrP^{Sc} (F4–6 red lines) versus the ferritin-containing fractions (F10–13). The relative amount of apparent α-helix and β-sheet character is reduced in the ferritin-depleted 22A-F4–6 when compared to the unfractionated 22A-Un and increased in F10–13. The dashed vertical lines indicate regions associated with α-helix (1652cm^{-1}) and β-sheet (1621–1631cm^{-1}) secondary structure.

Table 1

Protein identifications from mouse 22A and 79A enriched PrP^{Sc}.

79A-PrP^{Sc}-associated proteins (Uniprot ID)	Spectral Counts	Unique Peptides	mw (kDa)	% Coverage	Mock
Major Prion protein (P04925)	443	31	27.9	57.5	
Ferritin light chain 1 (P29391)	395	16	20.8	67.2	√
Ferritin heavy chain (P09528)	202	17	21.0	66.5	√
Apolipoprotein E (P08226)	95	20	35.8	50.5	
Myelin proteolipid protein (P60202)	31	6	30.0	17.0	
Gap junction alpha-1 protein (P23242)	31	6	43.0	19.6	
Tubulin chains [1]	19	11	-	-	
Myelin-associated oligodendrocyte basic protein (Q9D2P8)	18	3	19.2	14.7	
Collagen alpha-2(I) chain (Q01149)	13	4	129.5	3.8	√
Collagen alpha-1(I) chain (P11087)	11	3	137.9	2.5	√
Polyubiquitin-B (P0CG49)	9	2	34.3	5.6	
Pyruvate dehydrogenase E1 component α, mitochondrial (P35486)	6	2	43.2	5.6	
60S ribosomal protein L15 (Q9CZM2)	4	3	24.1	16.2	
ADP/ATP translocase 1 (P48962)	4	2	32.9	8.4	
Glyceraldehyde-3-phosphate dehydrogenase (P16858)	4	2	35.8	7.2	
Hemoglobin subunit beta-2 (P02089)	2	2	15.9	18.4	

22A-PrP^{Sc}-associated proteins (Uniprot ID)	Spectral Counts	Unique Peptides	mw (kDa)	% Coverage	Mock
Major Prion protein (P04925)	664	35	27.9	55.9	
Ferritin light chain 1 (P29391)	337	19	20.8	76.0	√
Ferritin heavy chain (P09528)	228	18	21.0	66.5	√
Tubulin chains [1]	52	21	NA	NA	
Pyruvate dehydrogenase complex component E2 (Q8BMF4)	51	8	67.9	15.6	
Myelin proteolipid protein (P60202)	31	4	30.0	16.6	
Gap junction alpha-1 protein (P23242)	25	4	43.0	11.0	
Glyceraldehyde-3-phosphate dehydrogenase (P16858)	14	3	35.8	11.7	
Apolipoprotein E (P08226)	13	5	35.8	18.3	
Guanine nucleotide-binding protein subunit beta-2 (P62880)	8	2	37.3	6.5	
Actin, cytoplasmic 1 (P60710)	7	4	41.7	10.9	
Vesicle-fusing ATPase (P46460)	5	2	82.5	3.2	
Ras-related protein Rab-3A (P63011)	5	2	24.9	9.5	
Dihydropyrimidinase-related protein 2 (O08553)	5	2	62.2	4.9	
2',3'-cyclic-nucleotide 3'-phosphodiesterase (P16330)	5	2	47.1	5.2	
Ca/calmodulin-dependent protein kinase type II subunit α (P11798)	4	2	54.1	5.0	
Prolow-density lipoprotein receptor-related protein 1 (Q91ZX7)	3	2	504.4	0.5	
Syntaxin-binding protein 1 (O08599)	3	2	67.5	1.9	
60S ribosomal protein L18 (P35980)	2	2	21.6	13.8	

All proteins listed in Table 1 were calculated with a 1% false discovery rate threshold and were identified by at least two unique peptides as described in methods. Keratin and trypsin sequences were filtered from the list. Proteins within a sample group are listed in order of relative apparent abundance based upon their spectral counts. A checkmark indicates that the protein was also found in mock preparations.

[1] Tubulin chains and subunits are listed cumulatively. A complete list is provided as supplemental material.

Table 2

Protein identification from enriched hamster 263K PrP^{Sc}.

263K-PrP^{Sc}-associated proteins (Uniprot ID)	Spectral Counts	Unique Peptides	mw (kDa)	% coverage	Mock
Major Prion protein (P04273)	7369	80	27.9	57.5	
Ferritin heavy chain[1]	915	39	~20	65.6	√
Ferritin light chain[1]	404	13	~20	38.8	√
60S ribosomal subunits[2]	419	83	-	-	√
Apolipoprotein E[1]	305	17	18.1	54.7	
Myelin proteolipid protein (P60202)	141	5	30.0	12.3	√
Myelin-associated oligodendrocyte basic protein (Q63327)	82	5	19.1	26.5	
Polyubiquitin-C (P0CG50)	39	3	82.5	5.7	
Collagen alpha-1(I) chain (P02454)	36	9	137.9	11.2	√
60 kDa heat shock protein, mitochondrial (P18687)	29	23	60.9	41.4	
Histone H4 (P62804)	29	5	11.3	52.4	√
40S ribosomal protein S6 (P62754)	26	4	28.6	21.7	
DNA (cytosine-5)-methyltransferase 1 (P13864)	23	4	183.1	3.0	
ADP/ATP translocase 1 (P48962)	15	6	32.9	23.2	√
Glyceraldehyde-3-phosphate dehydrogenase (P51640)	10	6	33.5	16.0	
V-type proton ATPase 16 kDa proteolipid subunit (P63081)	9	5	15.8	25.2	√
Tuftelin-interacting protein 11 (Q5U2Y6)	9	5	96.1	10.2	
Macrophage-expressed gene 1 protein (A1L314)	9	3	78.3	5.9	
Collagen alpha-2(I) chain (Q01149)	8	5	129.5	7.5	√
ADP/ATP translocase 2 (P51881)	6	4	32.9	14.1	√
Proteasome subunit alpha type-2 (P17220)	6	3	25.9	16.7	
Reticulon-3 (Q9ES97)	6	3	103.8	5.5	
Claudin-11 (aQ60771)	5	4	22.1	15.9	√
Myosin-Va (Q9QYF3)	5	4	211.6	2.5	
Myosin-Id (Q5SYD0)	4	3	116.0	4.5	√
Exocyst complex component 6 (O54923)	4	4	93.1	6.8	
Prenylcysteine oxidase (Q9CQF9)	3	3	56.4	12.7	

All proteins listed in Table 2 were calculated below a 1% false discovery rate and were identified by at least three unique peptides as described in methods. Keratin and trypsin sequences were filtered from the list. Proteins are listed in order of relative apparent abundance based upon their spectral counts. A checkmark indicates that the protein was also found in mock preparations.

[1]Ferritin and apolipoprotein E sequences are hamster-specific and the others were matched against Uniprot sequences with *rodentia* taxonomy.

[2]Ribosomal 60S subunits are listed cumulatively. A comprehensive list of all the proteins and peptides is provided as supplemental material.

Table 3

Protein identifications from uninfected hamster and mouse preparations.

Mock-sample associated proteins (Uniprot ID)	Mo/Ha[1]	Spectral Counts	Unique Peptides	% coverage
Ferritin heavy chain (P09528)	Mo	135	24	48.9
Ferritin light chain 1 (P29391)	Mo	68	18	67.8
Collagen alpha-1(I) chain (P11087)	Mo	22	6	5.0
V-type proton ATPase proteolipid subunit (P63082)	Mo	15	15	19.4
Collagen alpha-2(I) chain (Q01149)	Mo	8	6	6.9
Myelin-associated oligodendrocyte basic protein[2] (Q9D2P8)	Mo	2	2	7.6
Ferritin heavy chain[3]	Ha	213	20	47.2
60S ribosomal subunits[4]	Ha	171	-	-
V-type proton ATPase proteolipid subunit (P63081)	Ha	72	9	19.4
Myelin proteolipid protein (P60202)	Ha	59	5	15.5
Ferritin light chain[3]	Ha	55	7	33.51
2'3'-cyclic-nucleotide 3'-phosphodiesterase (P16330)	Ha	53	9	20.7
Histone H4 (P62804)	Ha	51	8	54.4
Collagen alpha-1(I) chain (P02454)	Ha	38	9	9.0
Gap junction alpha-1 protein (P08050)	Ha	21	4	14.1
Collagen alpha-2(I) chain (Q01149)	Ha	16	6	5.3
ADP/ATP translocase 1 (P48962)	Ha	7	3	11.7
Ca/calmodulin-dependent protein kinase type II-α (P11275)	Ha	5	4	9.2

All proteins listed were calculated at or below a 1% false discovery rate as described in methods. Keratin and trypsin sequences were filtered from the list. Proteins are listed in order of relative apparent abundance based upon their spectral counts.

[1] Mo represents mouse proteins, Ha refers to identifications from hamster samples.

[2] With the exception of myelin-associated oligodendrocyte basic protein, proteins were identified by ≥3 unique peptides.

[3] Ferritin was identified from hamster-specific sequences as described in methods. Other proteins were matched against Uniprot sequences with *rodentia* taxonomy.

[4] Ribosomal subunits are listed cumulatively. A complete list is provided as supplemental material.